Plant Communications, Volume *1*

Supplemental Information

Abscisic Acid Connects Phytohormone Signaling with RNA Metabolic Pathways and Promotes an Antiviral Response that Is Evaded by a Self-Controlled RNA Virus

Fabio Pasin, Hongying Shan, Beatriz García, Maren Müller, David San León, Márta Ludman, David H. Fresno, Károly Fátyol, Sergi Munné-Bosch, Guillermo Rodrigo, and Juan Antonio García

SUPPLEMENTAL METHODS

Transcriptomic analysis of *Nicotiana benthamiana* samples

Raw RNA-seq reads were filtered with Trimmomatic (Bolger et al., 2014) to remove poor quality reads and adapter contaminations. The remaining reads were mapped to the *Nicotiana benthamiana* transcriptome (Transcriptome assembly v5, primary transcripts (Nakasugi et al., 2014)) using Bowtie2 (Langmead and Salzberg, 2012) with the very-sensitive option activated. Transcript read counts were obtained by RSEM software (Li and Dewey, 2011), and rRNA counts were discarded. Differential expression analysis was calculated with edgeR and false discovery rates (FDR; Dataset_S1A) were computed by the Benjamini–Hochberg method (Robinson et al., 2010). Viral reads were mapped to a full-length PPV genome using HISAT2 (Kim et al., 2015); single nucleotide coverage was obtained using the igvtools `count` command (Thorvaldsdóttir et al., 2013). Cluster analyses were done using ClustVis (Metsalu and Vilo, 2015); when indicated, approximately unbiased and bootstrap *p* values were calculated by bootstrap resampling (1000 or 10000 replications) using Pvclust (Suzuki and Shimodaira, 2006). Gene list overlaps were visualized using euler*APE* (Micallef and Rodgers, 2014) and intersection plots were generated using UpSetR (Conway et al., 2017). Significance of gene list overlaps was determined by the hypergeometric test (upper cumulative distribution).

Gene functional annotations

To identify *Arabidopsis thaliana* homologs, *N. benthamiana* transcripts were used to search an *A. thaliana* protein database (TAIR10_pep_20101214_updated) with BLASTX (*e* value < 0.1); *N. benthamiana PR* transcripts were annotated on the basis of known *PR* genes (Dataset_S1B). Gene ontology (GO) classes associate to TAIR loci (version November 18, 2018) were obtained from the GO Consortium database [(The Gene Ontology Consortium, 2017); http://www.geneontology.org/gene-associations/]. TAIR loci associated to the GO:0003700 term were identified as transcription factors. GO classes containing "gene silencing" or "sirna" were searched in AmiGO [http://amigo.geneontology.org/amigo/search/ontology], and were used to identify gene silencing loci. GO classes containing the term "salicylic" were used to identify loci associated to salicylic acid; classes were filtered to remove those containing the terms "not depend upon salicylic acid signaling". The AgriGO webserver (Tian et al., 2017) was used to determine GO classes overrepresented within gene lists. Enrichment significance of GO terms was determined by Fisher's exact test and Hochberg correction.

Quantification of alternative splice events in *Arabidopsis thaliana* samples

Raw RNA-seq reads from time series ABA experiments (Song et al., 2016) were retrieved (SRP073711), and filtered with Trimmomatic (Bolger et al., 2014) to remove poor quality reads and adapter contaminations. The AtRTD2-QUASI (version AtRTDv2_QUASI_19April2016.fa), a high-quality *A. thaliana* transcriptome, was used as a reference (Zhang et al., 2017). Salmon 1.2.1 (Patro et al., 2017) was used for indexing using the `-keepDuplicates -k 31` options, and a *A. thaliana* Col-0 genome sequence obtained from ENSEMBL as a decoy. Isoform read counts were obtained by Salmon in the mapping-based mode, including the `--validateMappings --seqBias` options. Splice event coordinates were retrieved from AtRTDv2_QUASI_19April2016.gtf (Zhang et al., 2017) using SUPPA 2.1 (Trincado et al., 2018). The SUPPA `psiPerEvent` and `diffSplice` (including the `-m empirical -gc` options, and the `-th 1` filter as described (Love et al., 2018)) were used to identify differential alternative splicing events and event types; an adjusted $p < 0.05$ was used as a significance threshold (Dataset_S1D).

Generation of an augmented transcriptome assembly of *N. benthamiana* and its use in differential expression and splice analysis of RNA-seq samples

A reference genome dataset including host and viral sequences was obtained from the draft assembly Niben.genome.v1.0.1.contigs.fasta.gz of *N. benthamiana* genome (Bombarely et al., 2012), the pSN-PPV vector and the *nahG* gene (GenBank: M60055) sequences. *N. benthamiana* transcripts from Nbv5.1_transcriptome_primary_alternate_correct.fa.gz and NbDE transcriptome datasets (Nakasugi et al., 2014; Kourelis et al., 2019) were mapped to the reference genome dataset using Minimap2 in the splice mode (Li, 2018); gtf files were retrieved using StringTie with the `-R` option (Pertea et al., 2015). Transcripts from P1Pro- and PPV-infected *N. benthamiana* plants were obtained as described (Pertea et al., 2016). Briefly, raw RNA-seq reads were filtered with Trimmomatic (Bolger et al., 2014), mapped using the spliced aligner HISAT2 with the --dta option (Kim et al., 2015) against the reference genome dataset. Gtf files were retrieved using StringTie, which was used in the merge mode to obtain a final gtf file including transcript annotations from reference transcriptomes and those assembled from P1Pro- and PPV-infected samples. A padded version of transcript sequences was obtained using GffRead with `--w-add 200 -w` options (Zhang et al., 2017; Pertea and Pertea, 2020); this augmented transcriptome assembly of *N. benthamiana* was used in differential expression and splice analysis in P1Pro- and PPV-infected samples (Datasets S1F to S1H). Transcripts were quantified by Salmon (Patro et al., 2017); gene-level differential expression analysis was performed using tximport and EdgeR (Robinson et al., 2010; Soneson et al., 2015); Cook's distance filtering was used to remove genes with outliers. Differential alternative splicing events and event types were identified by SUPPA 2.1 as described above (Dataset_S1H).

Mathematical model

A mathematical model based on four ordinary differential equations (ODE) was developed to describe the dynamics of plum pox virus in plants. The amounts of potyviral RNA (denoted by *R*), potyviral polyprotein (*Q*), potyviral processed protein (*P*), and host protein of the immune system (*S*) were considered as variables. The host plant (or a part of it, a leaf) was assumed as a single, uniform compartment in which the virus can replicate. Sigmoidal expressions were used to model the different biochemical processes underlying such replication following a generalized enzyme kinetics scheme in which both substrates and enzymes are limited in the medium (Rodrigo et al., 2011a). Parameter values are provided in Table S3.

In first place, the ODE for *R* reads

$$\frac{dR}{dt} = k_{syn}\frac{PR}{(\theta + P + R)(1 + S)}\left(1 - \frac{R}{K}\right) - k_{sil}\frac{R^2}{\psi + \alpha P + R},$$

where two different terms were considered to construct it. The first term accounts for the synthesis of more potyviral RNA using the available molecules as a template through the action of viral replication proteins. This synthesis depends on both potyviral RNA and potyviral processed protein; k_{syn} is the viral RNA synthesis rate (in this case) and was assumed to be $k_{syn} = 3$ h^{-1} (i.e., three new viral genomes per hour), taking the same order of magnitude as in the case of an RNA virus infecting animals (Dahari et al., 2007). θ represents the protein-RNA dissociation constant, taking here $\theta = 20$ mol. That is, about 20 molecules of viral replication proteins are required to start the virus replication. The rate is nonetheless limited, on the one hand by the availability of resources, which we modeled in a logistic way. K denotes the maximal host resources available and its value was set to $K = 10^7$ mol, following a previous estimate (Martínez et al., 2011). On the other hand, viral RNA replication was assumed to be limited by action of the immune system (modeled by *S*). To simulate viral fitness after alteration of the RNA synthesis rate, the value of k_{syn} was adjusted by the correction factor τ, i.e. in the ODE for *R* we replaced k_{syn} by τk_{syn}.

The second term accounts for potyviral RNA degradation by the action of the RNA silencing machinery. The k_{sil} is the RNA silencing rate, here assumed to be $k_{sil} = 3$ h^{-1}, following the quantification in *Drosophila* (Haley and Zamore, 2004). This degradation depends on the amount of viral RNA, as well as potyviral processed protein (mostly HCPro, the viral suppressor of silencing). In our model, ψ represents the RNA silencing threshold; i.e., the amount of potyviral RNA from which the RNA silencing machinery starts. We empirically established $\psi = 10^4$ mol. When the amount of potyviral RNA is high enough ($R >> \psi$), this rate can be considered at first order ($k_{sil}R$). The presence of the viral suppressor of silencing increases this threshold, as this protein is able to block that machinery. We modeled this by correcting the value of ψ by αP, where α denotes the strength of suppression ($\alpha = 0.1$ for a strong suppressor and $\alpha < 0.1$ for a weak suppressor).

In second place, the ODE for Q reads

$$\frac{dQ}{dt} = k_{syn}R - \delta Q \, ,$$

where only two simple terms (of first order) were considered. The first accounts for the production, and the second for the degradation. In this case, k_{syn} is the protein synthesis rate (i.e., three new potyviral polyproteins per hour). Note then that we assumed equal transcription and translation rates for simplicity. Moreover, δ is the protein degradation rate. In *A. thaliana*, rapidly-degrading proteins (as viral proteins are assumed to be) have half-lives of about one day (Li et al., 2017), so we took $\delta = 0.02$ h^{-1}.

In third place, the ODE for P reads

$$\frac{dP}{dt} = k_{clv} \frac{H}{1+H} \left(f_{clv} Q - P \right) - \delta P \, ,$$

where the first part of the right-hand side accounts for the cleavage process of the potyviral polyprotein, which is host-dependent. k_{clv} is the potyviral polyprotein cleavage rate, here assumed to be $k_{clv} = 60$ h^{-1} (i.e., a very rapid process that takes on average just 1 min), in agreement with previous characterizations (Carrington et al., 1989). The process is not completed in totality, however, meaning that a small but significant fraction of polyproteins remains unaffected even at long times. We modeled this fact by introducing f_{clv}, the fraction of cleaved protein at the equilibrium (f_{clv} = 0.7). The cleavage rate is therefore maximal at initial times and then decreases progressively (as long as *P* increases). In addition, *H* denotes the amount of a yet-unknown host factor essential for cleavage. This factor then limits the speed of the polyprotein processing. Here, we took $H = 0.001$ to model the wild-type virus scenario. The last part of the right-hand side, as before, corresponds to protein degradation. Note then that, for simplicity, we assumed equal polyprotein and protein degradation rates.

In fourth place, the ODE for *S* (which represents a protein amount normalized to the corresponding protein-DNA dissociation constant; perhaps a value close to θ) reads

$$\frac{dS}{dt} = k_{im}\left(\frac{P^n}{(\chi e^{\delta t})^n + P^n} + \frac{S^n}{1 + S^n}\right) - \delta S\,,$$

where one term composed of two subterms corresponds to the synthesis rate of the immune system protein and the last term corresponds to the degradation of that protein. For simplicity, we took the same degradation rate as before (δ). Production of the immune system protein is dependent on the presence of the potyviral processed protein in an amount sufficient to be sensed by the plant cell (modeled by the first subterm). In our model, χ represents the transcriptional threshold of the immune system; i.e., the amount of potyviral processed protein (*e.g.*, HCPro, CI, NIb, CP, etc.) from which the immune system machinery starts; empirically, we set $\chi = 10^8$ mol. The longer the time, however, the harder it is for the plant to mount this response, as the virus has more time to inhibit and/or subvert the host elements. Because of this extreme, we corrected the value of χ by a temporal exponential factor. In addition, the defense response was assumed to be maintained active once it has been mounted, through the action of positive feedback (modeled by the second subterm). k_{im} is the maximal synthesis rate of *S*. We considered $k_{im} = 0.2$ h^{-1}, leading to protein amounts similar to those previously considered to model a gene regulatory network in plants (Rodrigo et al., 2011b). Finally, *n* denotes the Hill coefficient of this regulation (here, $n = 4$).

Numerical simulations to obtain viral infection dynamics were carried out with MATLAB (MathWorks). Different scenarios (corresponding to different virus clones) were modeled by changing key parameter values. For example, to model an HCPro mutant, we replaced $\alpha = 0.1$ with $\alpha = 0$ (i.e., no suppression); to model a clone lacking the P1 autoinhibitory domain (P1Pro) and its uncontrolled self-cleavage, we replaced $H = 0.001$ with $H \to \infty$ (i.e., host-independent cleavage).

SUPPLEMENTAL FIGURES

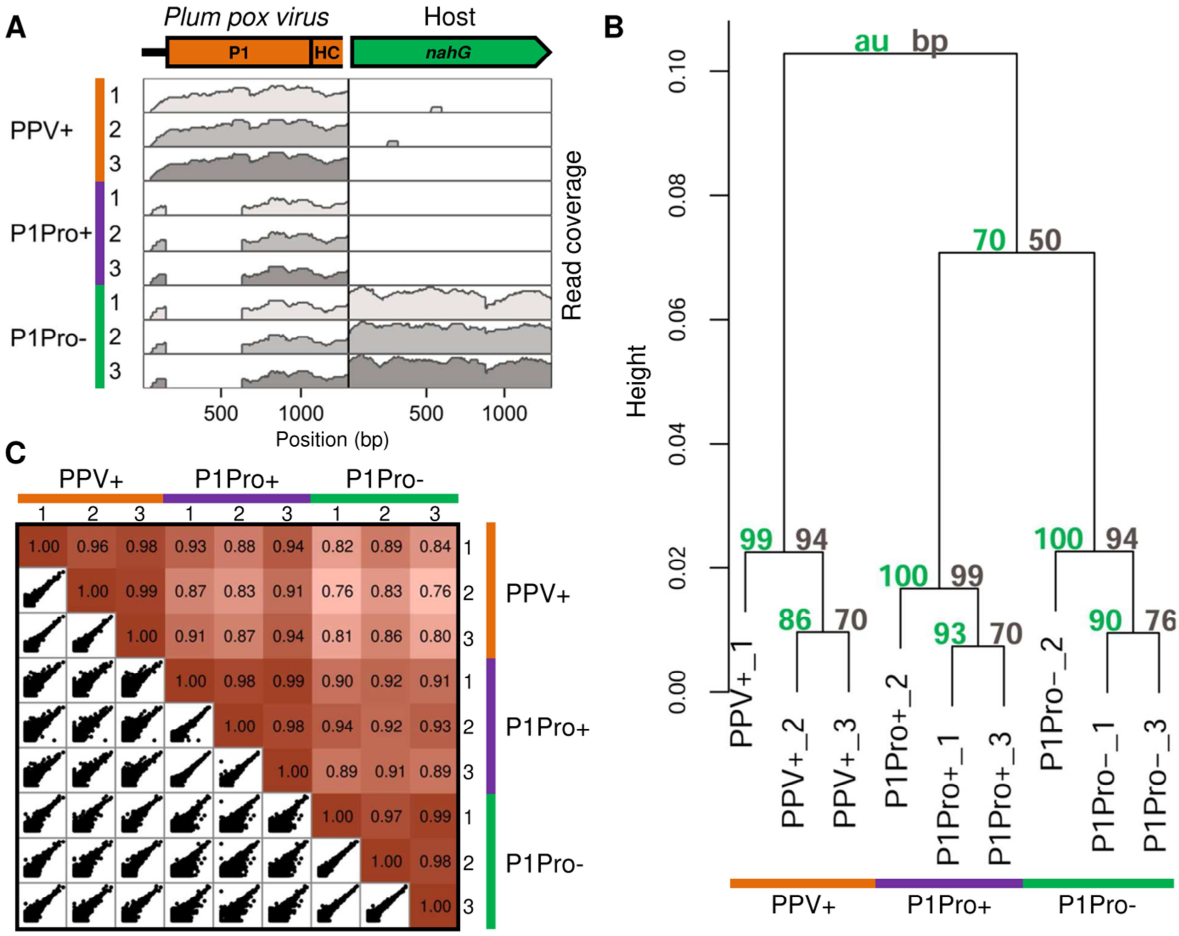

Supplemental Figure 1. Quality control of RNA-seq samples.

(A) Read coverage (log10 scale) of the 5' terminus of the PPV genome and coding sequence of the *nahG* transgene (GenBank: M60055).

(B) Confidence of the unsupervised multivariate analysis and sample grouping shown in Figure 1C. Clustering dendrogram and probability values are indicated (au, approximately unbiased; bp, bootstrap probability).

(C) Correlation values and plots of the biological replicates analyzed by RNA-seq. Counts of differentially regulated transcripts (FDR < 0.05 in two-way comparisons) in at least one comparison were used to compute Pearson's *r* values.

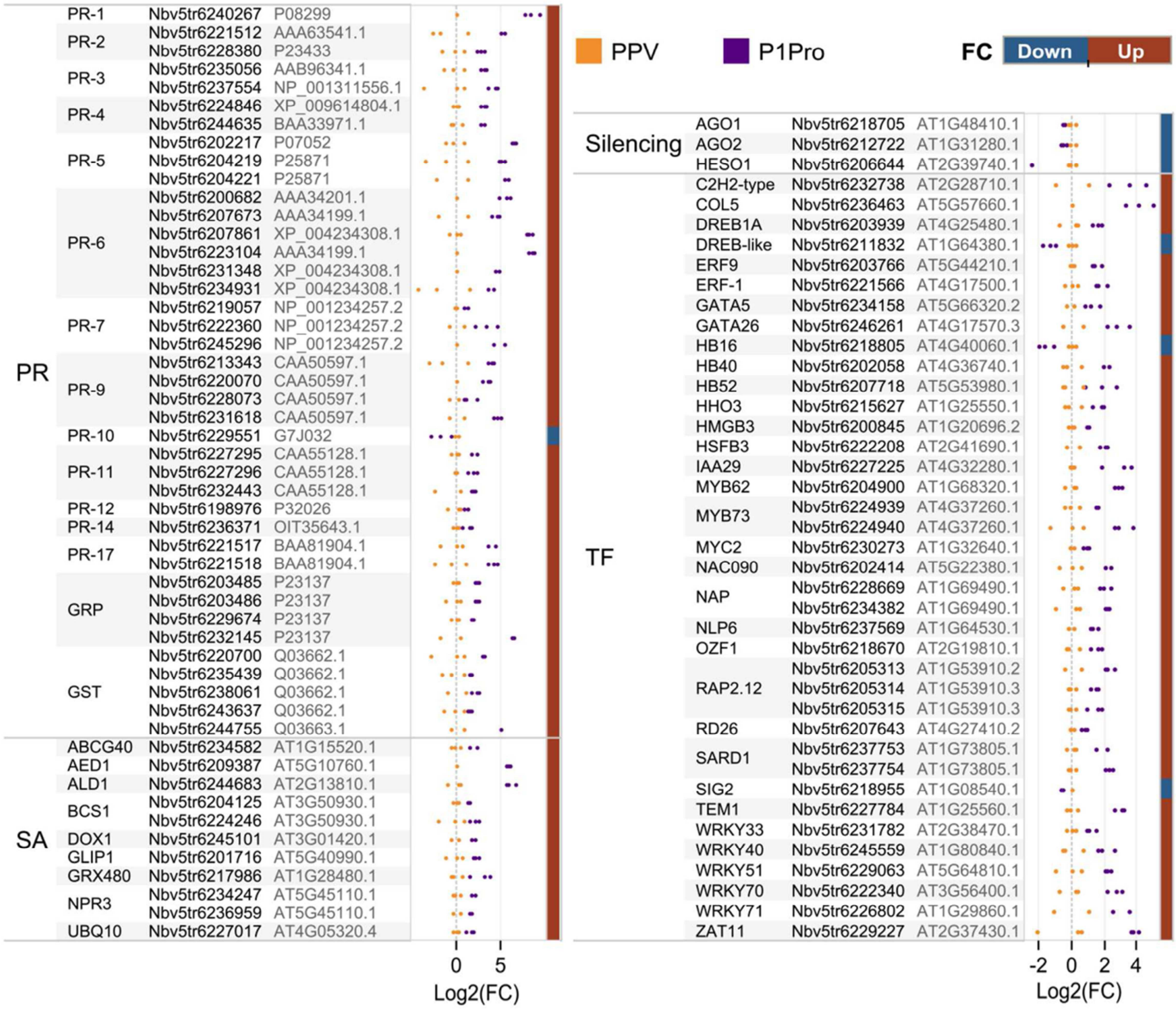

Supplemental Figure 2. Defense marker and transcription factor genes differentially regulated by P1Pro with respect to PPV.

Functional annotation of differentially expressed transcripts of wild-type *N. benthamiana* plants infected with PPV or P1Pro was carried out by searching known pathogenesis-related protein (PR) and *Arabidopsis thaliana* sequences; SA, salicylic acid-related genes; Silencing, RNA silencing genes; TF, transcription factors. For each transcript, the symbol, the accession codes of the *N. benthamiana* gene, and reference homologs are indicated; expression values using PPV mean value as reference are plotted for each biological replicate (n = 3), and colored according to the experimental condition analyzed (PPV, orange; P1Pro, purple); red or blue boxes highlight up- or downregulated transcripts, respectively; only transcripts with an FDR < 0.01 are shown.

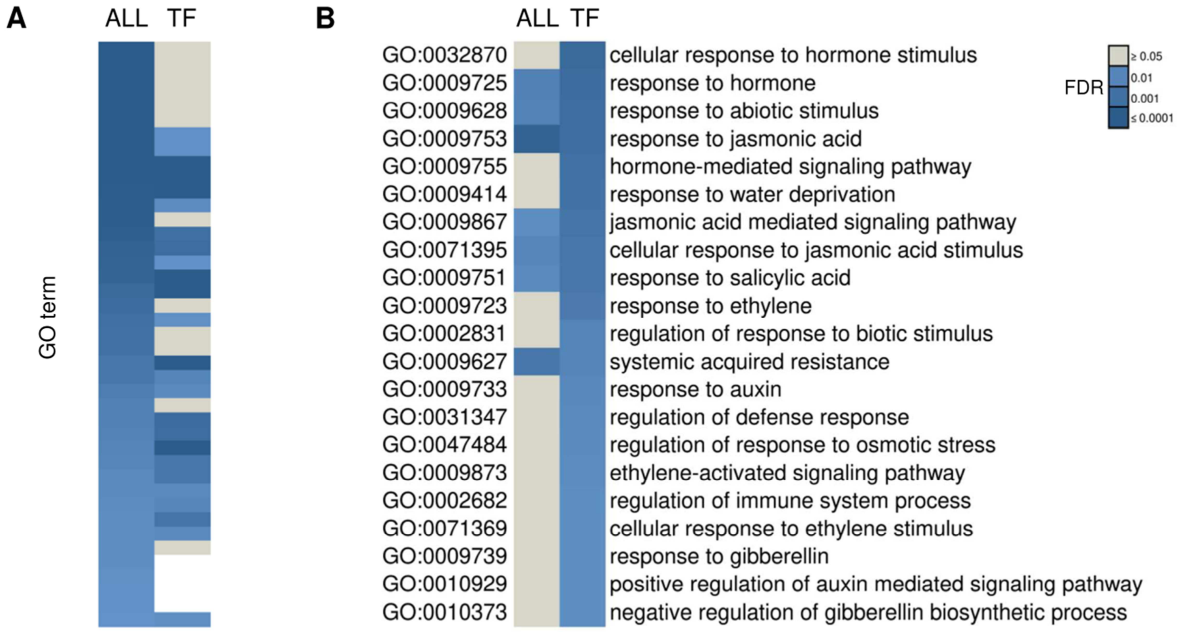

Supplemental Figure 3. Enrichment of functional categories in genes differentially regulated by P1Pro with respect to PPV.

Differentially expressed transcripts (FDR < 0.05) of wild-type *N. benthamiana* plants infected with PPV or P1Pro (P1Pro+/PPV+ comparison) were analyzed.

(A) Significance value of gene ontology (GO) terms enriched in the differentially expressed transcripts (ALL transcripts); the GO significance value is also shown for the subset including only genes encoding transcription factors (TF).

(B) GO terms enriched in the TF subset along with their significance value by ALL transcript analysis. Color scale shows enrichment significance by Fisher's exact test with Hochberg's FDR correction.

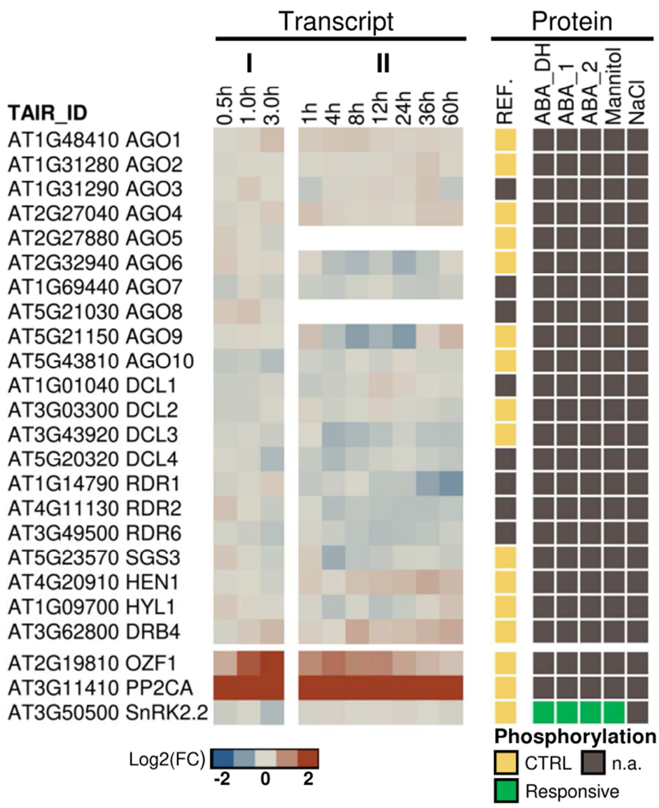

Supplemental Figure 4. Transcriptional and post-translational effects of ABA on the antiviral RNA silencing.

Right, *A. thaliana* accession numbers of the major antiviral RNA silencing components. Center, time-course analysis of transcript fold-changes in *A. thaliana* seedlings treated with ABA; I, microarray study (Nemhauser et al., 2006); II, RNA-seq study (Song et al., 2016). Right, phosphorylation responsiveness of RNA silencing protein after ABA and dehydration (ABA_DH), ABA (ABA_1, ABA_2), mannitol or NaCl treatments (Umezawa et al., 2013; Wang et al., 2013; Wang et al., 2020); a comprehensive phosphoproteome dataset (REF.) was used as a control of known phophoproteins (Mergner et al., 2020). *OZF1* and *PP2CA* are included as ABA-inducible transcript controls; SnRK2.2 as a protein of which phosphorylation status is ABA responsive.

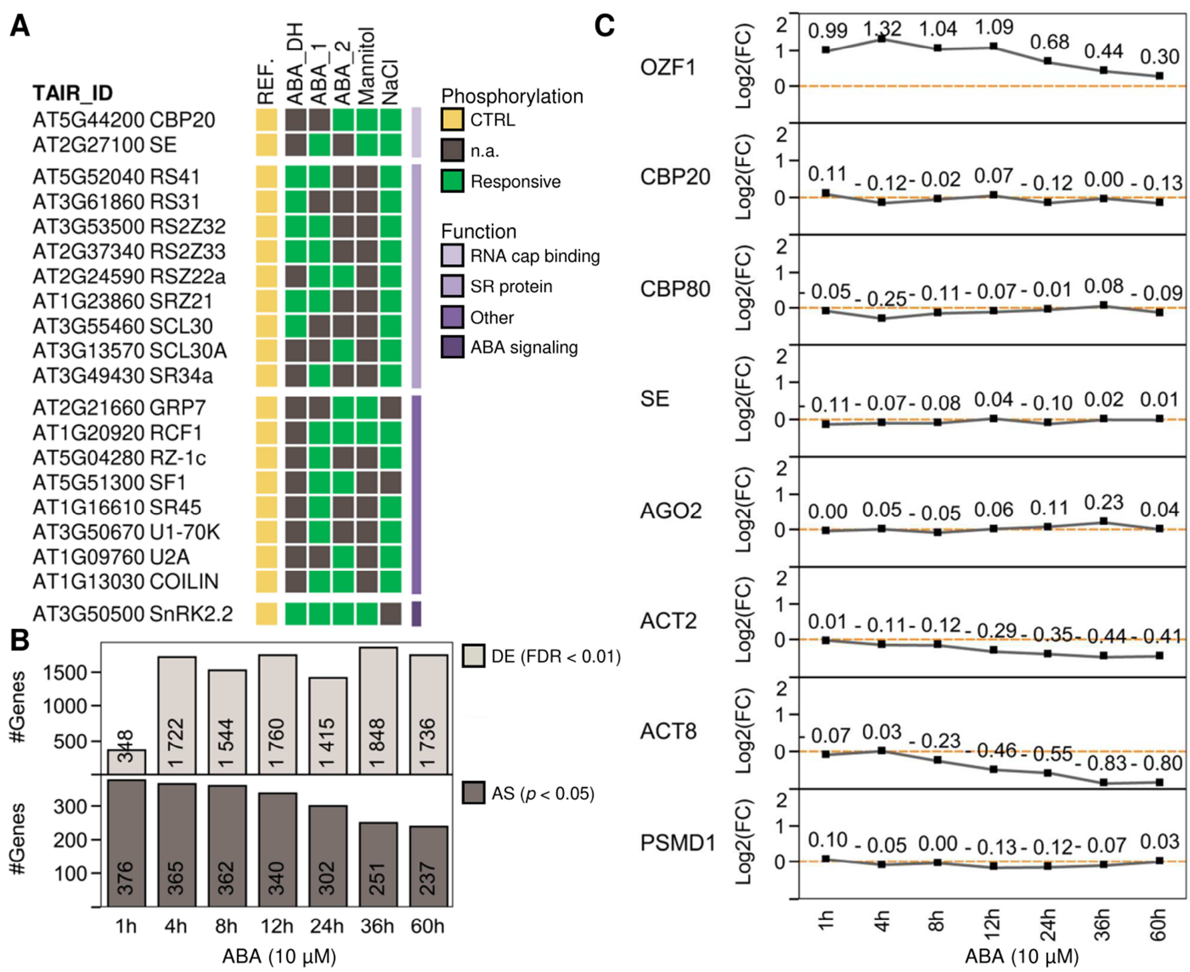

Supplemental Figure 5. ABA-dependent regulation of host mRNA splicing.

(A) Phosphorylation responsiveness of *A. thaliana* proteins implicated in constitutive and alternative splicing after ABA and dehydration (ABA_DH), ABA (ABA_1, ABA_2), mannitol or NaCl treatments (Umezawa et al., 2013; Wang et al., 2013; Wang et al., 2020); a comprehensive phosphoproteome dataset (REF.) was used as a control of known phophoproteins (Mergner et al., 2020). Serine/arginine-rich (SR) splicing factors were annotated according to Barta et al. (2010); SnRK2.2, protein of which phosphorylation status is ABA responsive.

(B) Time-course analysis of genes differentially expressed (DE, FDR < 0.01), and genes with alternative splicing events significantly altered (AS, $p < 0.05$) in *A. thaliana* seedlings treated with ABA.

(C) Time-course, ABA-dependent transcriptional regulation of selected genes in *A. thaliana*. Fold-changes are shown of an ABA-inducible transcript (OZF1, AT2G19810), components

 https://doi.org/10.1016/j.xplc.2020.100099

(CBP20, AT5G44200; CBP80, AT2G13540) or interactors (SE, AT2G27100) of the nuclear cap-binding complex, an RNA silencing gene (AGO2, AT1G31280), reference genes commonly used in RT-qPCR assays (ACT2, AT3G18780; ACT8, AT1G49240), and a gene whose abundance show small fluctuations under ABA treatment (PSMD1, AT2G32730). Time series RNA-seq data were used (Song et al., 2016).

Correspondence: fpasin@cnb.csic.es

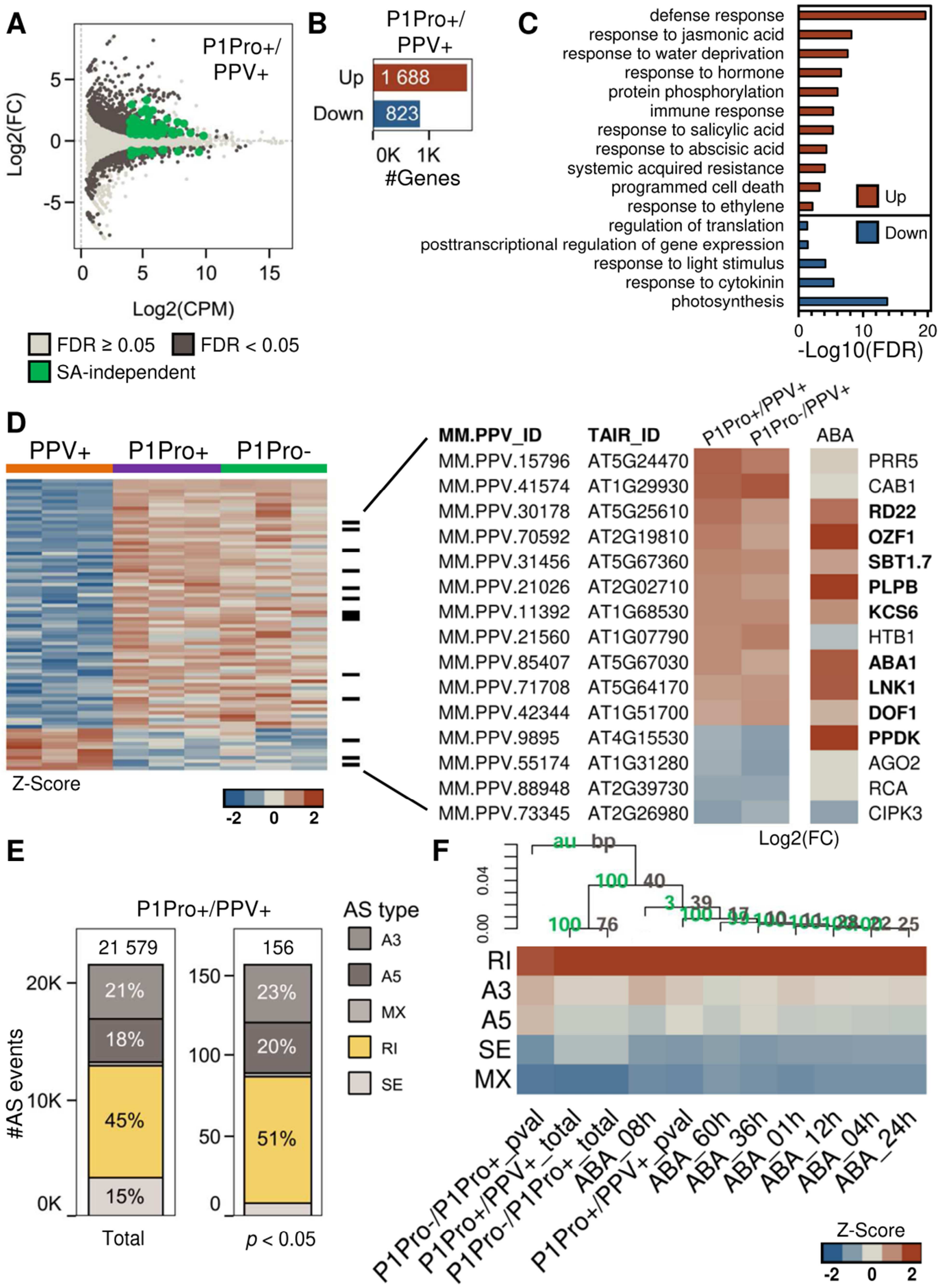

Supplemental Figure 6. An augmented transcriptome assembly of *N. benthamiana* enhanced the analysis of P1Pro-induced responses.

RNA-seq reads from P1Pro and PPV-infected *N. benthamiana* plants were used for *de novo* assembly of host transcripts. The transcriptome obtained was merged with reported datasets, and used in gene expression and splice event analysis of wild-type *N. benthamiana* plants agroinoculated with PPV (PPV+) or P1Pro clones (P1Pro+), and *nahG*-expressing plants with P1Pro (P1Pro-).

(A) Gene-level fold-changes and coverage values of the P1Pro+/PPV+ transcriptomic comparison. Differentially expressed genes are marked (FDR < 0.05); the green dots indicate a subset of genes that are altered in P1Pro-infected wild-type plants, but not in *nahG*-transgenic plants (where SA signaling is down-regulated; i.e., SA-independent genes).

(B) Number of differentially expressed genes identified in the P1Pro+/PPV+ comparison.

(C) Selected GO terms enriched in genes up- or down-regulated in the P1Pro+/PPV+ comparison.

(D) Left, normalized read counts (heatmap; n = 3) of the SA-independent gene subset. Right, representative genes from the SA-independent subset and their fold-changes in the P1Pro+/PPV+ or P1Pro-/PPV+ comparisons are shown along with expression values of their *A. thaliana* homologs after ABA treatment (Nemhauser et al., 2006).

(E) Alternative splice (AS) events identified in the P1Pro+/PPV+ comparison. Ratios of AS types are plotted: SE, skipping exon; RI, retained intron; MX, mutually exclusive exon; A5, alternative 5' splice site; A3, alternative 3' splice site. AS event numbers and type ratios are shown for all the events identified (Total) or only those significantly altered (adjusted $p < 0.05$).

(F) Hierarchical clustering of normalized ratios of the AS types identified by analysis of our samples, or RNAseq data from ABA-treated *A. thaliana* plants; cluster probabilities are indicated (au, approximately unbiased; bp, bootstrap probability).

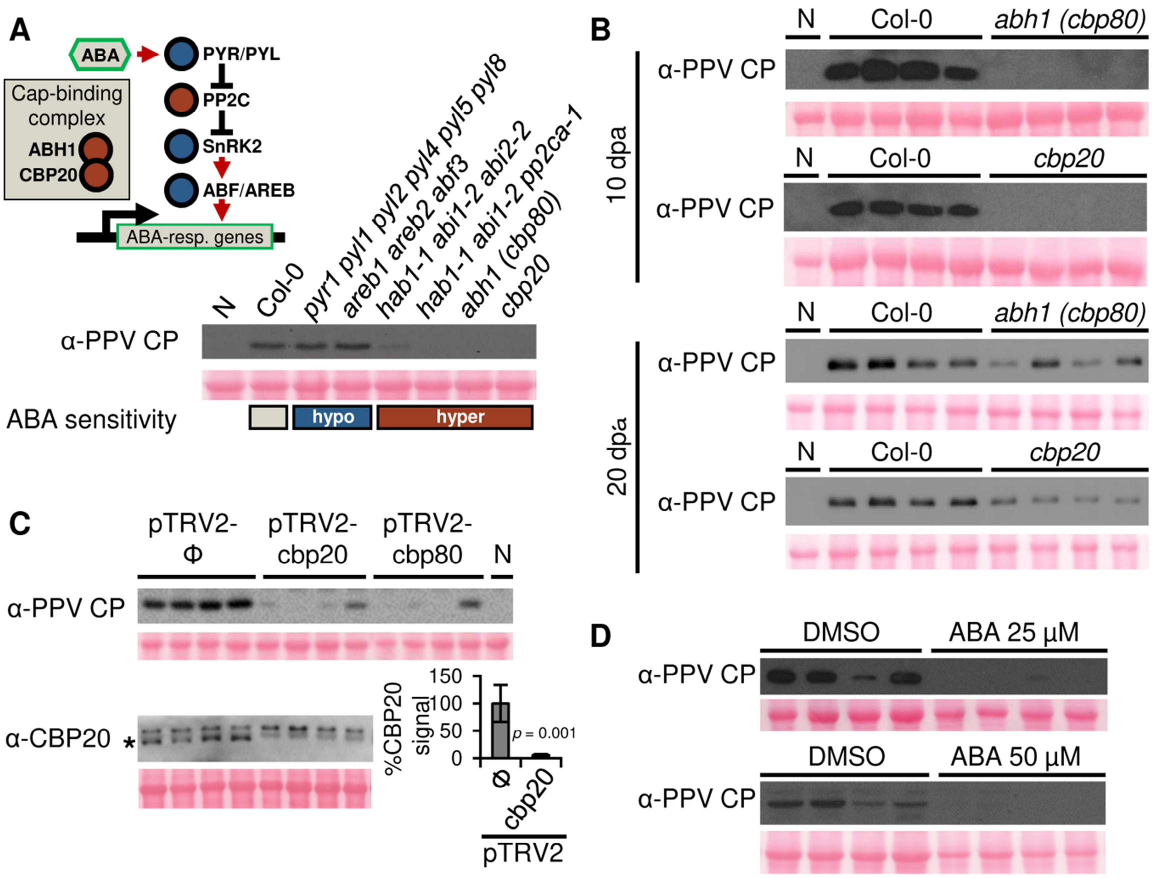

Supplemental Figure 7. ABA and RNA metabolic defects promote resistance to plum pox virus (PPV).

(A) Top, diagram of ABA signaling components; arrows and T-bars indicate positive and negative interactions, respectively. Bottom, immunoblot shows PPV coat protein (CP) accumulation in *A. thaliana* mutant lines at 14 days post agro-inoculation (dpa); the Col-0 accession and its mutant lines *pyr1 pyl1 pyl2 pyl4 pyl5 pyl8* (Gonzalez-Guzman et al., 2012), *areb1 areb2 abf3* (Yoshida et al., 2010), *hab1-1 abi1-2 abi2-2* and *hab1-1 abi1-2 pp2ca-1* (Rubio et al., 2009), *abh1(cbp80)* (Hugouvieux et al., 2001), and *cbp20* (Papp et al., 2004) were used. ABA perception of the lines screened is indicated: hypo- (blue) and hypersensitive (red); N, non-treated sample.

(B) PPV accumulation in *A. thaliana abh1(cbp80)* and *cbp20* lines at 10 and 20 dpa. Anti-PPV CP immunoblots are shown; for quantification values, see Figure 5A.

(C) VIGS of cap-binding complex genes in *N. benthamiana*. The pTRV2-cbp20 or pTRV2-cbp80 vectors were delivered to target *NbCBP20* and *NbCBP80* transcripts, respectively; pTRV2-Φ, empty vector control. TRV-treated plants were inoculated with PPV. The anti-PPV CP

Correspondence: fpasin@cnb.csic.es

 https://doi.org/10.1016/j.xplc.2020.100099

immunoblot is shown; for quantification values, see Figure 5D. Bottom, immunoblot using anti-CBP20 serum. The asterisk marks a major band that is absent in pTRV2-cbp20 samples; band quantification is plotted (mean ± SD, $n = 4$); p value is indicated (Student's t test); N, non-treated sample.

(D) PPV accumulation after ABA treatments. Anti-PPV CP immunoblot of samples from plants treated with 25 µM ABA or DMSO solutions; for quantification values, see Figure 5E. Anti-PPV CP immunoblot of samples from plants treated with 50 µM ABA or DMSO solutions. Ponceau red-stained blots are shown as loading controls.

Correspondence: fpasin@cnb.csic.es

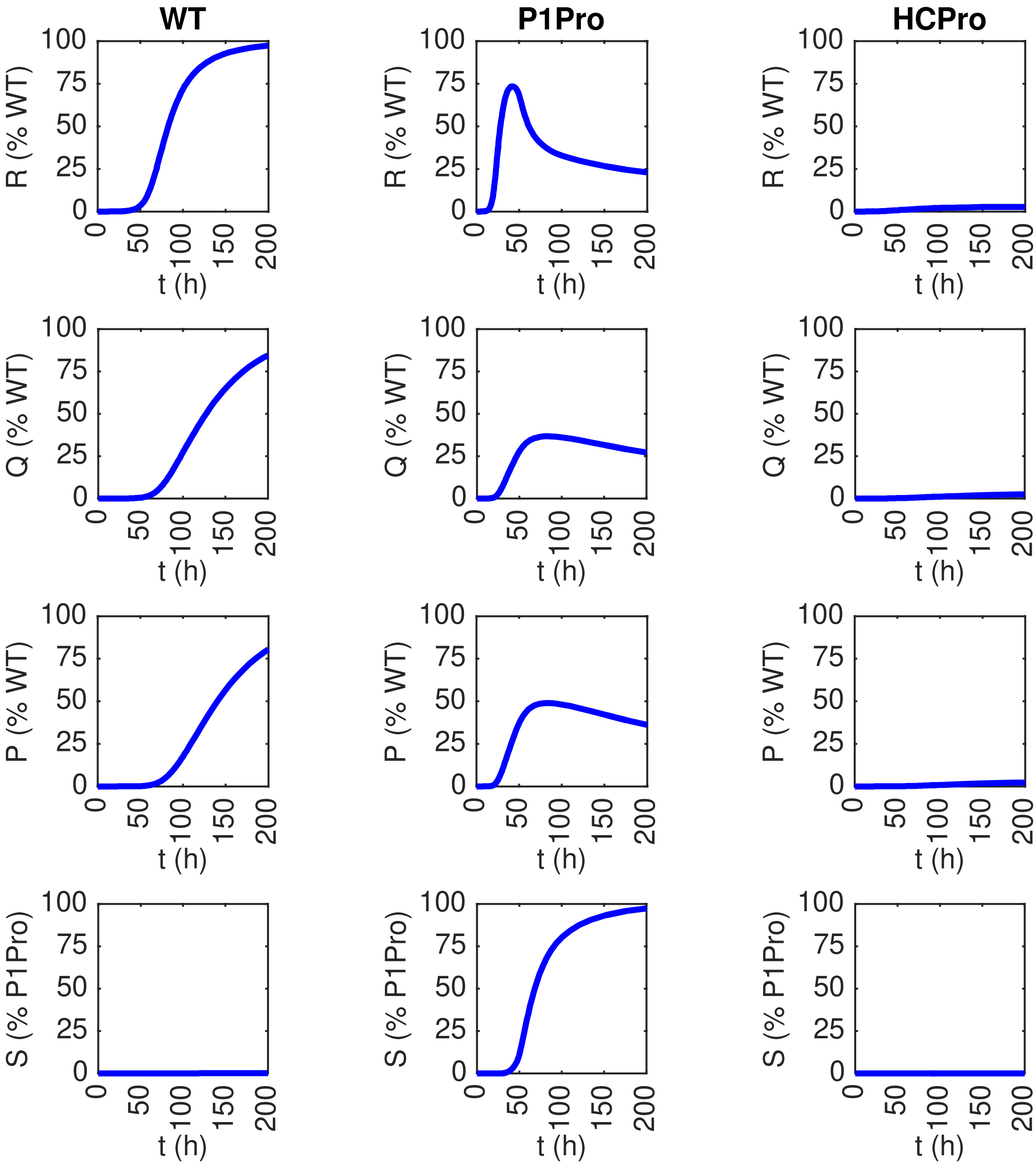

Supplemental Figure 8. Simulations of infection dynamics.

Virus RNA (*R*), potyviral polyprotein (*Q*), potyviral processed protein (*P*), and host protein of the immune system (S) are plotted for scenarios of three different clones: self-controlled, wild-type PPV (WT, left); a clone lacking the P1 autoinhibitory domain and with uncontrolled self-cleavage (P1Pro, center); and a mutant clone with an HCPro with no suppression activity (HCPro, right).

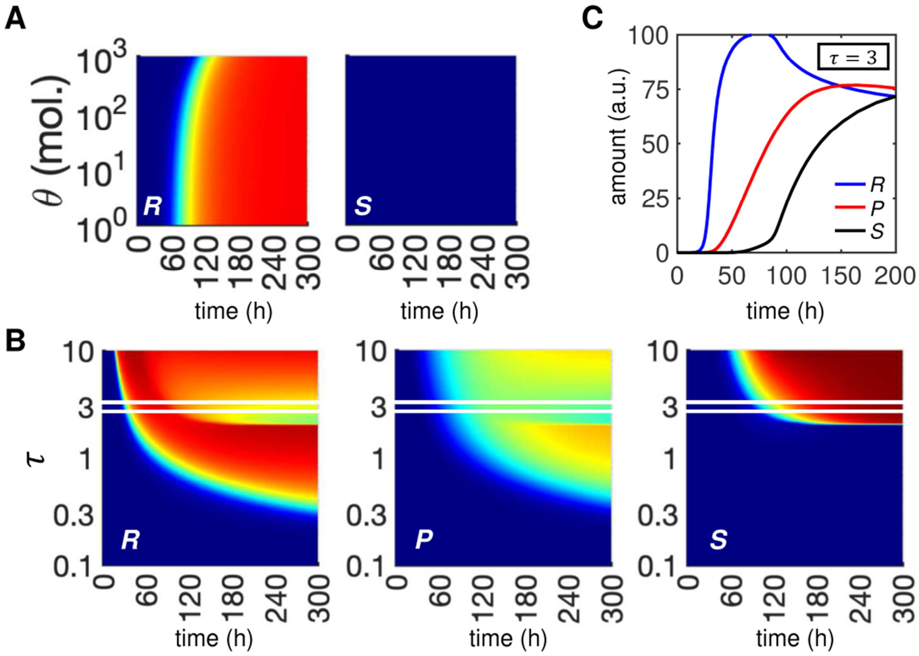

Supplemental Figure 9. Simulations of viral load and immune response dynamics for varying efficiency of viral replication.

Dynamics were modeled for varying RNA binding constant (θ) of the viral replicase or for the viral RNA synthesis rate (k_{syn}) adjusted by the correction factor τ (i.e. τk_{syn}). Numerical simulations of viral RNA (*R*), mature protein (*P*) and immune response (*S*) levels are shown for the wild-type PPV scenario, i.e. the virus clone with a self-controlled polyprotein processing.

(A) Time-course simulations of the *R*, and *S* accumulation relative to the maximum (dark blue for 0% and dark red for 100%) are shown for varying RNA binding constant (θ) of the replicase.

(B) Time-course simulations of the *R*, *P*, and *S* accumulation relative to the maximum (dark blue for 0% and dark red for 100%) are shown for varying RNA synthesis rate. The $\tau = 3$ value is marked and its dynamics are plotted in panel C. (**C**) The *R*, *P*, and *S* dynamics for $\tau = 3$.

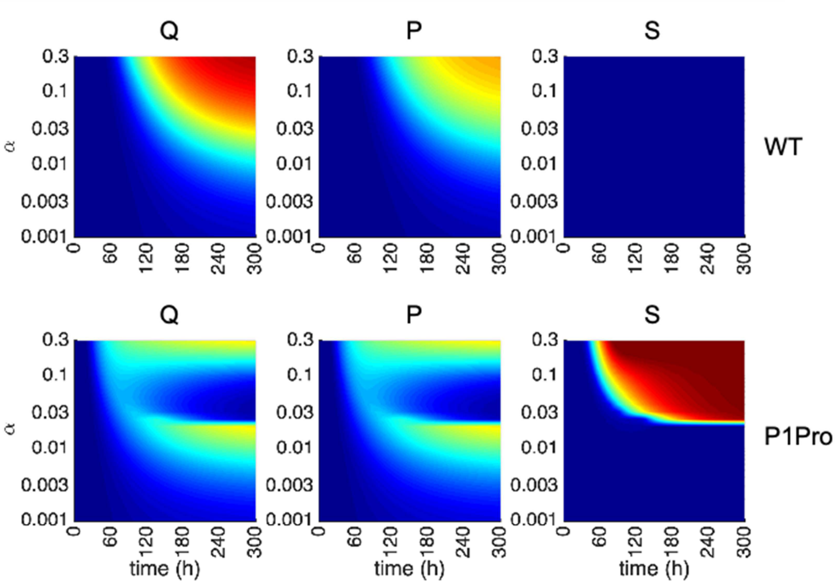

Supplemental Figure 10. Simulations of expression dynamics for varying strength of suppression.

Time-course simulations of viral polyprotein (*Q*) and mature protein (*P*), and immune response (*S*) levels are shown as % relative to the maximum; dark blue for 0% and dark red for 100%. The wild-type PPV (WT, top), and the uncontrolled self-cleavage (P1Pro, bottom) scenarios are shown; α, strength of the RNA silencing suppression.

SUPPLEMENTAL TABLES

Supplemental Table 1. Salicylic acid-independent genes differentially expressed in P1Pro+/PPV+ and P1Pro-/PPV+ comparisons

Transcript*			P1Pro+/PPV+		P1Pro-/PPV+	
SYDNEY_ID#	TAIR_ID	TAIR_Symbol	Log2(FC)	FDR	Log2(FC)	FDR
Nbv5tr6236463	AT5G57660	COL5	6.32	1.0E-03	6.10	5.3E-03
Nbv5tr6208832	n.a.	n.a.	4.19	5.9E-14	4.18	2.3E-13
Nbv5tr6199225	AT2G07777	n.a.	3.54	3.6E-40	3.56	8.2E-39
Nbv5tr6226581	n.a.	n.a.	2.09	1.3E-18	2.09	1.1E-12
Nbv5tr6241923	AT1G29930	CAB1	1.86	2.3E-14	2.16	2.3E-12
Nbv5tr6243964	n.a.	n.a.	1.77	6.5E-05	1.84	1.5E-04
Nbv5tr6236418	AT5G24470	PRR5	1.59	7.4E-08	1.31	3.3E-04
Nbv5tr6236294	AT1G29930	CAB1	1.58	1.7E-07	2.19	8.0E-10
Nbv5tr6206822	n.a.	n.a.	1.49	9.2E-03	1.51	1.4E-02
Nbv5tr6218670	AT2G19810	OZF1	1.40	1.6E-06	1.02	1.3E-02
Nbv5tr6207355	AT1G29930	CAB1	1.33	5.2E-09	1.83	5.1E-12
Nbv5tr6212008	AT5G66150	n.a.	1.28	3.0E-05	1.08	7.2E-03
Nbv5tr6215695	n.a.	n.a.	1.27	4.5E-15	0.93	8.0E-05
Nbv5tr6218584	AT1G06760	H1.1	1.25	3.4E-02	1.47	2.9E-02
Nbv5tr6236371	AT1G27950	LTPG1	1.24	6.8E-03	1.41	6.9E-03
Nbv5tr6216301	n.a.	n.a.	1.21	1.8E-03	1.29	7.3E-03
Nbv5tr6236193	AT5G25610	RD22	1.12	7.1E-07	0.67	2.4E-02
Nbv5tr6206135	AT1G29930	CAB1	1.12	2.1E-05	1.84	1.9E-11
Nbv5tr6198976	AT1G61070	LCR66	1.04	2.3E-03	1.32	6.7E-05
Nbv5tr6204947	AT2G02710	PLPB	1.02	8.3E-07	0.83	1.4E-03
Nbv5tr6229630	AT2G05070	LHCB2.2	1.00	1.2E-02	1.67	3.4E-08
Nbv5tr6219057	AT5G67360	SBT1.7	1.00	5.7E-05	1.04	1.9E-04
Nbv5tr6241941	AT2G34430	LHB1B1	0.95	5.4E-05	1.63	1.0E-12
Nbv5tr6233144	AT4G37800	XTH7	0.87	1.4E-03	1.25	3.6E-10
Nbv5tr6241860	AT1G29930	CAB1	0.83	2.2E-02	1.05	3.1E-02
Nbv5tr6226195	AT1G68530	KCS6	0.83	2.0E-02	0.87	2.4E-02
Nbv5tr6241423	AT1G07790	HTB1	0.76	4.3E-02	1.01	2.9E-03
Nbv5tr6245715	ATMG01190	ATP1	0.63	2.2E-09	0.37	7.9E-03
Nbv5tr6206813	ATMG00090	RPS3	0.47	1.0E-02	0.41	3.0E-03
Nbv5tr6212722	AT1G31280	AGO2	-0.66	7.6E-03	-0.88	5.0E-04
Nbv5tr6230075	AT4G15530	PPDK	-0.68	5.2E-03	-0.92	7.4E-03
Nbv5tr6236236	ATCG01250	NDHB.2	-1.03	3.4E-06	-0.76	9.4E-03
Nbv5tr6202574	AT5G17100	n.a.	-1.18	4.6E-06	-0.97	1.1E-03
Nbv5tr6230855	ATCG00490	RBCL	-1.21	1.9E-02	-1.35	3.9E-05
Nbv5tr6246056	ATCG00720	PETB	-1.21	3.0E-02	-1.57	6.3E-03
Nbv5tr6202627	AT1G30760	ATBBE-LIKE 13	-1.23	2.3E-05	-0.75	4.3E-02
Nbv5tr6200121	ATCG00680	PSBB	-1.39	4.7E-05	-1.02	3.4E-02
Nbv5tr6241933	AT1G47128	RD21A	-2.27	3.5E-02	-4.17	2.8E-03
Nbv5tr6221690	AT4G13010	CEQORH	-6.29	1.4E-02	-6.20	3.7E-02

*n.a., not applicable; no TAIR gene with BLASTX *e* value < 0.1, or no gene symbol available
#Accession numbers of *N. benthamiana* transcripts (Nakasugi et al., 2014)

Supplemental Table 2. AGO2 tryptic peptide quantification in PPV and P1Pro-infected plant samples

Protein		Peptide					Quantification*			
SYDNEY_ID	Symbol	Sequence	Modification	mz[#]	z[#]	m[#]	PPV 115	PPV 117	P1Pro 114	P1Pro 116
Nbv5tr6212722	AGO2	(R)DVQPNSSEASTVR(Q)	iTRAQ4plex	767.38	2	1532.75	0.00	0.02	-1.19	-0.60

*Biological replicates (n = 2) were labeled with the iTRAQ tag indicated (PPV, 115 and 117; P1Pro, 114 and 116). Quantification values are expressed in Log2(FC) using the 115-tagged PPV sample as a reference.
[#]Experimental

Supplemental Table 3. Summary of parameter values used for mathematical modeling

Parameter	Value	Parameter	Value
k_{syn}	3 h^{-1}	k_{sil}	3 h^{-1}
θ	20 mol.	ψ	10^4 mol.
K	10^7 mol.	α	0.1 0 (HCPro)
δ	0.02 h^{-1}	H	0.001 ∞ (P1Pro)
k_{clv}	60 h^{-1}	f_{clv}	0.7
k_{im}	0.2 h^{-1}	n	4
χ	10^8 mol.		

Supplemental Table 4. Plasmids used in the study

ID	Description	Reference
pSN-PPV	Infectious clone of a GFP-tagged plum pox virus (PPV) isolate adapted to *Nicotiana* spp., and suitable for *Agrobacterium*-mediated infection	(Pasin et al., 2014)
pSN-PPV P1Pro[V164]	pSN-PPV-based clone with the truncated P1 lacking residues 2-163 (herein, the P1Pro clone)	(Pasin et al., 2014)
pGr208	Potato virus X (PVX) infectious clone	(Peart et al., 2002)
pTRV1	TRV RNA1 vector (YL192)	(Liu et al., 2002)

pTRV2-Φ	TRV RNA2 silencing vector (also known as pTRV2-MCS or YL156; GenBank:AF406991)	(Liu et al., 2002)
pBTEX::avrPtoB	Binary vector for transient expression of the HopAB2 (AvrPtoB) effector from the *Pseudomonas syringae* pv. tomato DC3000 strain	(Kim et al., 2002)
pSN.5 P1|HC-Stop	Binary vector for transient expression of the full-length PPV P1 and HCPro cistrons, and flanked by PPV 5' and 3' UTRs	(Pasin et al., 2014)
pSN.5 P1Pro|HC-Stop	Binary vector for transient expression of a PPV P1 version lacking residues 2-163, the full-length HCPro cistron, and flanked by PPV 5' and 3' UTRs	(Pasin et al., 2014)
pSN.5 P1Pro-Stop	Binary vector for transient expression of a PPV P1 version lacking the 2-163 residues, no HCPro cistron, and flanked by PPV 5' and 3' UTRs	This study
pSN.5 AvrPtoB#3	Binary vector for transient expression of a version of the HopAB2 effector flanked by PPV 5' and 3' UTRs; subcloned from the pBTEX::avrPtoB	This study
pTRV2-cbp20	TRV RNA2 silencing vector including a cDNA fragment of the *N. benthamiana* Nbv5tr6270933 gene (*NbCBP20*). Plant total RNA was used in RT-PCR reactions; a 442-bp fragment of *NbCBP20* was amplified using X277_F/X278_R primers and inserted into the XmaI/XbaI-digested pTRV2-Φ vector by one-step isothermal assembly (Gibson et al., 2009) to yield pTRV2-cbp20.	This study
pTRV2-cbp80	TRV RNA2 silencing vector including a cDNA fragment of the *N. benthamiana* Nbv5tr6236567 gene (*NbCBP80*). Plant total RNA was used in RT-PCR reactions; a 426-bp fragment of *NbCBP80* was amplified using X275_F/X276_R primers, and inserted into the XmaI/XbaI-digested pTRV2-Φ vector by one-step isothermal assembly (Gibson et al., 2009) to yield pTRV2-cbp80.	This study

Supplemental Table 5. Sequences of the primers used

ID	Sequence*	Use
X275_F	ccgtagtttaatgtcttcgggacatgCATATTACACATTGGTTATCATCG	Cloning
X276_R	gattctgtgagtaaggttaccTaattctCCTTTCACCATGTCCTTCAGC	Cloning
X277_F	ccgtagtttaatgtcttcgggacatgCTGTCAAAcATATCAGCGGGAC	Cloning
X278_R	gattctgtgagtaaggttaccTaattCTCTCACGGAAACGTGGATT	Cloning
2174_F	CCTTAATTTCTCTACCAAATTTACTGC	RT-PCR
1631_R	GCACAAGAACTATAACCCGAATGG	RT-PCR
REF_1_F	GCTGCTCTAGGAACTGCTGATGA	RT-qPCR
REF_1_R	TACCTtGTGCCAAACCCCTGAT	RT-qPCR
CBP20_F	TCGTGCTGGAGAGATTAAAAAGATAGT	RT-qPCR
CBP20_R	CGAATAGGGCGATCATCAAGAA	RT-qPCR
CBP80_F_1095	AGAGTATTTGTTGGATGTGCTTTTATT	RT-qPCR
CBP80_R_1277	GCCCCTGcCAGAGCCTTG	RT-qPCR
OZF1_F	AGCCCATCAACATTCCGACC	RT-qPCR
OZF1_R	CCTTCCAGATTCTACCCTCTCCAT	RT-qPCR

*Mismatched nucleotides in lower case

Supplemental Table 6. Gene-specific primers used in qRT-PCR assays

SYDNEY_ID	TAIR_ID	Symbol	Forward	Reverse	Product size
Nbv5tr6218939	AT2G32730	NbPSMD1	REF_1_F	REF_1_R	202bp
Nbv5tr6270933	AT5G44200	NbCBP20	CBP20_F	CBP20_R	153bp
Nbv5tr6236567	AT2G13540	NbCBP80	CBP80_F_1095	CBP80_R_1277	207bp
Nbv5tr6218670	AT2G19810	NbOZF1	OZF1_F	OZF1_R	144bp

Supplemental Table 7. Sequences of the *N. benthamiana* cDNA fragments used in VIGS assays

Construct	Sequence*
pTRV2-cbp20	ctgtgagtaaggttacctaattCTCTCACGGAAACGTGGATTCTTCTCCGGTCTGGACTCGTGATCA GAGTTTCTTCGAGATTCACGGTCATAACTCCTCTTTGGATAATCTGACCGATGGCGGTCATCTTCCC TGTGTCGCTTGCGTTGATAGTCTCTACCGTGTCGATAAGAACCTCCATGACCTTGATTTCCACCATG TCTACCATAGTGAGGTGGCGGCATAACCGGTGGGTAACCGCCCAATGATCCTGTACCATAATCCACT AGCTGCCTTTGTGCTTCCAACTCCTTTTGGACCAATTTTCCATAACCACCTCGACCTGGATCGTAGT CAGTACGATATTCGTCGCGCACCTGTCCACCACTCCTACCACGGCCCCATTGCCTACCTTCTTGAAA TCCCCAGTCAAAATCCACACGAATAGGGCGATCATCAAGAATTGTCCCGCTGATATGTTTGACAGca tgtcccgaagacattaaactac
pTRV2-cbp80	ctgtgagtaaggttacctaattctCCTTTCACCATGTCCTTCAGCTCTACAGAGAGTGCACGCTCAG TTGGATCTGTACCATCTTCTGCACTATATTTAAACTGTGGTCCACCTCTCGGTGGAAGTAACTCCTC CAAAGCAGGGGTGTTCTCAATGCTCTGCTTGATTTTGTCCCAATATGAAAGACGGACTTCTCTTTCC AAAACCTCTTGAACAAACACACGCTGTGGGGCCCATTTTGGCAGATCTAACACATGAGCCCATTCTT CCCATGGCCAGATAAATTGAAAGTTTGACAAATGATGTGAGAACCAAAGGATGAGACGTGTTCGGCA TTCCATGTCTAAATCTGCTATTTTATCAAAAAGAGCACGGACAGCCCCAGCTACAACCGCTGGAAAG GCCCCTGGCAGAGCCTTGCATAAATCGATGATAACCAATGTGTAATATGcatgtcccgaagacatta aactac

*Upper case, *N. benthamiana* cDNA sequence cloned; lower case, pTRV2 vector sequence

SUPPLEMENTAL REFERENCES

Barta, A., Kalyna, M., and Reddy, A. S. N. (2010). Implementing a rational and consistent nomenclature for serine/arginine-rich protein splicing factors (SR proteins) in plants. *Plant Cell* 22:2926–2929.

Bolger, A. M., Lohse, M., and Usadel, B. (2014). Trimmomatic: a flexible trimmer for Illumina sequence data. *Bioinforma. Oxf. Engl.* 30:2114–2120.

Bombarely, A., Rosli, H. G., Vrebalov, J., Moffett, P., Mueller, L. A., and Martin, G. B. (2012). A draft genome sequence of *Nicotiana benthamiana* to enhance molecular plant-microbe biology research. *Mol. Plant. Microbe Interact.* 25:1523–1530.

Carrington, J. C., Freed, D. D., and Sanders, T. C. (1989). Autocatalytic processing of the potyvirus helper component proteinase in *Escherichia coli* and in vitro. *J. Virol.* 63:4459–4463.

Conway, J. R., Lex, A., and Gehlenborg, N. (2017). UpSetR: an R package for the visualization of intersecting sets and their properties. *Bioinforma. Oxf. Engl.* 33:2938–2940.

Dahari, H., Ribeiro, R. M., Rice, C. M., and Perelson, A. S. (2007). Mathematical modeling of subgenomic hepatitis C virus replication in Huh-7 cells. *J. Virol.* 81:750–760.

Gibson, D. G., Young, L., Chuang, R.-Y., Venter, J. C., Hutchison III, C. A., and Smith, H. O. (2009). Enzymatic assembly of DNA molecules up to several hundred kilobases. *Nat. Methods* 6:343–345.

Gonzalez-Guzman, M., Pizzio, G. A., Antoni, R., Vera-Sirera, F., Merilo, E., Bassel, G. W., Fernández, M. A., Holdsworth, M. J., Perez-Amador, M. A., Kollist, H., et al. (2012). *Arabidopsis* PYR/PYL/RCAR receptors play a major role in quantitative regulation of stomatal aperture and transcriptional response to abscisic acid. *Plant Cell* 24:2483–2496.

Haley, B., and Zamore, P. D. (2004). Kinetic analysis of the RNAi enzyme complex. *Nat. Struct. Mol. Biol.* 11:599–606.

Hugouvieux, V., Kwak, J. M., and Schroeder, J. I. (2001). An mRNA cap binding protein, ABH1, modulates early abscisic acid signal transduction in *Arabidopsis*. *Cell* 106:477–487.

Kim, Y. J., Lin, N. C., and Martin, G. B. (2002). Two distinct *Pseudomonas* effector proteins interact with the Pto kinase and activate plant immunity. *Cell* 109:589–598.

Kim, D., Langmead, B., and Salzberg, S. L. (2015). HISAT: a fast spliced aligner with low memory requirements. *Nat. Methods* 12:357–360.

Kourelis, J., Kaschani, F., Grosse-Holz, F. M., Homma, F., Kaiser, M., and van der Hoorn, R. A. L. (2019). A homology-guided, genome-based proteome for improved proteomics in the alloploid *Nicotiana benthamiana*. *BMC Genomics* 20:722.

Langmead, B., and Salzberg, S. L. (2012). Fast gapped-read alignment with Bowtie 2. *Nat. Methods* 9:357–359.

Li, H. (2018). Minimap2: pairwise alignment for nucleotide sequences. *Bioinforma. Oxf. Engl.* 34:3094–3100.

Li, B., and Dewey, C. N. (2011). RSEM: accurate transcript quantification from RNA-Seq data with or without a reference genome. *BMC Bioinformatics* 12:323.

Li, L., Nelson, C. J., Trösch, J., Castleden, I., Huang, S., and Millar, A. H. (2017). Protein degradation rate in *Arabidopsis thaliana* leaf growth and development. *Plant Cell* 29:207–228.

Liu, Y., Schiff, M., Marathe, R., and Dinesh-Kumar, S. P. (2002). Tobacco *Rar1*, *EDS1* and *NPR1/NIM1* like genes are required for *N*-mediated resistance to tobacco mosaic virus. *Plant J.* 30:415–429.

Love, M. I., Soneson, C., and Patro, R. (2018). Swimming downstream: statistical analysis of differential transcript usage following Salmon quantification. *F1000Research* 7:952.

Martínez, F., Sardanyés, J., Elena, S. F., and Daròs, J.-A. (2011). Dynamics of a plant RNA virus intracellular accumulation: stamping machine vs. geometric replication. *Genetics* 188:637–646.

Mergner, J., Frejno, M., List, M., Papacek, M., Chen, X., Chaudhary, A., Samaras, P., Richter, S., Shikata, H., Messerer, M., et al. (2020). Mass-spectrometry-based draft of the *Arabidopsis* proteome. *Nature* 579:409–414.

Metsalu, T., and Vilo, J. (2015). ClustVis: a web tool for visualizing clustering of multivariate data using Principal Component Analysis and heatmap. *Nucleic Acids Res.* 43:W566-570.

Micallef, L., and Rodgers, P. (2014). eulerAPE: drawing area-proportional 3-Venn diagrams using ellipses. *PloS One* 9:e101717.

Nakasugi, K., Crowhurst, R., Bally, J., and Waterhouse, P. (2014). Combining transcriptome assemblies from multiple *de novo* assemblers in the allo-tetraploid plant *Nicotiana benthamiana*. *PloS One* 9:e91776.

Nemhauser, J. L., Hong, F., and Chory, J. (2006). Different plant hormones regulate similar processes through largely nonoverlapping transcriptional responses. *Cell* 126:467–475.

Papp, I., Mur, L. A., Dalmadi, A., Dulai, S., and Koncz, C. (2004). A mutation in the *Cap Binding Protein 20* gene confers drought tolerance to *Arabidopsis*. *Plant Mol. Biol.* 55:679–686.

Pasin, F., Simón-Mateo, C., and García, J. A. (2014). The hypervariable amino-terminus of P1 protease modulates potyviral replication and host defense responses. *PLOS Pathog.* 10:e1003985.

Patro, R., Duggal, G., Love, M. I., Irizarry, R. A., and Kingsford, C. (2017). Salmon provides fast and bias-aware quantification of transcript expression. *Nat. Methods* 14:417–419.

Peart, J. R., Cook, G., Feys, B. J., Parker, J. E., and Baulcombe, D. C. (2002). An *EDS1* orthologue is required for *N*-mediated resistance against tobacco mosaic virus. *Plant J.* 29:569–579.

Pertea, G., and Pertea, M. (2020). GFF utilities: GffRead and GffCompare. *F1000Research* 9:304.

Pertea, M., Pertea, G. M., Antonescu, C. M., Chang, T.-C., Mendell, J. T., and Salzberg, S. L. (2015). StringTie enables improved reconstruction of a transcriptome from RNA-seq reads. *Nat. Biotechnol.* 33:290–295.

Pertea, M., Kim, D., Pertea, G. M., Leek, J. T., and Salzberg, S. L. (2016). Transcript-level expression analysis of RNA-seq experiments with HISAT, StringTie and Ballgown. *Nat. Protoc.* 11:1650–1667.

Robinson, M. D., McCarthy, D. J., and Smyth, G. K. (2010). edgeR: a Bioconductor package for differential expression analysis of digital gene expression data. *Bioinforma. Oxf. Engl.* 26:139–140.

Rodrigo, G., Carrera, J., Jaramillo, A., and Elena, S. F. (2011a). Optimal viral strategies for bypassing RNA silencing. *J. R. Soc. Interface* 8:257–268.

Rodrigo, G., Jaramillo, A., and Blázquez, M. A. (2011b). Integral control of plant gravitropism through the interplay of hormone signaling and gene regulation. *Biophys. J.* 101:757–763.

Rubio, S., Rodrigues, A., Saez, A., Dizon, M. B., Galle, A., Kim, T.-H., Santiago, J., Flexas, J., Schroeder, J. I., and Rodriguez, P. L. (2009). Triple loss of function of protein phosphatases type 2C leads to partial constitutive response to endogenous abscisic acid. *Plant Physiol.* 150:1345–1355.

Soneson, C., Love, M. I., and Robinson, M. D. (2015). Differential analyses for RNA-seq: transcript-level estimates improve gene-level inferences. *F1000Research* 4:1521.

Song, L., Huang, S.-S. C., Wise, A., Castanon, R., Nery, J. R., Chen, H., Watanabe, M., Thomas, J., Bar-Joseph, Z., and Ecker, J. R. (2016). A transcription factor hierarchy defines an environmental stress response network. *Science* 354:aag1550.

Suzuki, R., and Shimodaira, H. (2006). Pvclust: an R package for assessing the uncertainty in hierarchical clustering. *Bioinforma. Oxf. Engl.* 22:1540–1542.

The Gene Ontology Consortium (2017). Expansion of the Gene Ontology knowledgebase and resources. *Nucleic Acids Res.* 45:D331–D338.

Thorvaldsdóttir, H., Robinson, J. T., and Mesirov, J. P. (2013). Integrative Genomics Viewer (IGV): high-performance genomics data visualization and exploration. *Brief. Bioinform.* 14:178–192.

Tian, T., Liu, Y., Yan, H., You, Q., Yi, X., Du, Z., Xu, W., and Su, Z. (2017). agriGO v2.0: a GO analysis toolkit for the agricultural community, 2017 update. *Nucleic Acids Res.* 45:W122–W129.

Trincado, J. L., Entizne, J. C., Hysenaj, G., Singh, B., Skalic, M., Elliott, D. J., and Eyras, E. (2018). SUPPA2: fast, accurate, and uncertainty-aware differential splicing analysis across multiple conditions. *Genome Biol.* 19:40.

Umezawa, T., Sugiyama, N., Takahashi, F., Anderson, J. C., Ishihama, Y., Peck, S. C., and Shinozaki, K. (2013). Genetics and phosphoproteomics reveal a protein phosphorylation network in the abscisic acid signaling pathway in *Arabidopsis thaliana*. *Sci. Signal.* 6:rs8.

Wang, P., Xue, L., Batelli, G., Lee, S., Hou, Y.-J., Van Oosten, M. J., Zhang, H., Tao, W. A., and Zhu, J.-K. (2013). Quantitative phosphoproteomics identifies SnRK2 protein kinase substrates and reveals the effectors of abscisic acid action. *Proc. Natl. Acad. Sci. U. S. A.* 110:11205–11210.

Wang, P., Hsu, C.-C., Du, Y., Zhu, P., Zhao, C., Fu, X., Zhang, C., Paez, J. S., Macho, A. P., Tao, W. A., et al. (2020). Mapping proteome-wide targets of protein kinases in plant stress responses. *Proc. Natl. Acad. Sci. U. S. A.* 117:3270–3280.

Yoshida, T., Fujita, Y., Sayama, H., Kidokoro, S., Maruyama, K., Mizoi, J., Shinozaki, K., and Yamaguchi-Shinozaki, K. (2010). AREB1, AREB2, and ABF3 are master transcription factors that cooperatively regulate ABRE-dependent ABA signaling involved in drought stress tolerance and require ABA for full activation. *Plant J.* 61:672–685.

Zhang, R., Calixto, C. P. G., Marquez, Y., Venhuizen, P., Tzioutziou, N. A., Guo, W., Spensley, M., Entizne, J. C., Lewandowska, D., Ten Have, S., et al. (2017). A high quality Arabidopsis transcriptome for accurate transcript-level analysis of alternative splicing. *Nucleic Acids Res.* 45:5061–5073.